# Laser-induced fluorescence study of collision-time asymmetry and speed-dependent effects on the $^{114}$Cd 326.1-nm line perturbed by Xe

A. Bielski, R. Ciuryło, J. Domysławska, D. Lisak, R. S. Trawiński, and J. Szudy
*Institute of Physics, Nicholas Copernicus University, Grudziądzka 5/7, PL-87-100 Toruń, Poland*
(Received 15 February 2000; published 17 August 2000)

Using a laser-induced fluorescence method detailed analysis of profiles of the $^{114}$Cd 326.1-nm line perturbed by xenon was performed, which revealed departures from the ordinary Voigt profile. These departures are shown to be consistent with fits of experimental profiles to a speed-dependent asymmetric Voigt profile. Coefficients of the pressure broadening, shift, and collision-time asymmetry are determined and compared with those calculated in the adiabatic approximation for the Czuchaj-Stoll potentials.

PACS number(s): 32.70.Jz, 33.70.−w, 34.20.−b

## I. INTRODUCTION

Profiles of pressure-broadened spectral lines at low densities of perturbing atoms are usually assumed in the form of a Lorentzian profile that is symmetric with respect to the position of the peak of the line. The full width at half maximum (FWHM) of the line and its collisional shift are linearly dependent on the perturber density. The use of Lorentzian profiles to interpret experimental data is justified for isolated lines if the collision duration can be neglected [1–3], i.e., when the impact approximation can be applied. In this approximation the collisions are assumed to be effectively instantaneous.

It was shown that if the finite duration of collision is taken into account, then the first-order correction term to the Lorentzian profile has a dispersion form [2–10] and it gives rise to the so-called ''collision-time asymmetry,'' which by now was measured only for a few spectral lines of a few elements perturbed by rare gases (see, e.g., [3] and references therein). It should be emphasized that as was indicated first by Berman [11] and later by many authors [12–14], all collisional parameters of the line profile, such as its width, shift and asymmetry are dependent on the emitter velocity.

The thermal motion of emitters leads to a well-known phenomenon of the Doppler-line broadening. In the case when the velocity-changing collisions can be neglected, which means that the emitter motion can be treated as a free motion (see also [14]) and the emitter velocity distribution is described by the Maxwellian distribution, the shape of the Doppler-broadened line can be given in the form of a Gaussian profile with the width dependent on the gas temperature and independent of the perturber density.

In the traditional analysis of line shapes, one assumes that the Doppler broadening is statistically independent of pressure broadening. In the impact limit, the combined influence of Doppler and pressure effects can be represented by the familiar Voigt profile (VP), which is a convolution of the Lorentzian and Gaussian profiles. Beyond the impact limit, i.e., in the case when the finite duration of collisions is taken into account, the resultant profile can be represented by the so-called asymmetric Voigt profile (AVP), which is the convolution of the Gaussian distribution with a sum of the Lorentzian and dispersion profiles.

The assumption of statistical independence of the Doppler broadening from the pressure effects is justified only in the case when the mass of the emitter $m_E$ is much greater than that of the perturber $m_P$: $m_E \gg m_P$. This means that for systems corresponding to very small values of $\alpha = m_P/m_E$, the ratio of perturber and emitter masses, the emitters are essentially stationary and all collisions are independent of the emitter velocity $\vec{v}_E$ so that either AVP or VP results, depending on whether the finite duration time of collisions is, respectively, taken into account or not.

With increasing values of $\alpha$, the assumption of statistical independence ceases to be valid, which means that the correlation between pressure broadening and velocity contributions to the line shape should be taken into account. Following Berman [11] and Ward *et al.* [12] this can be done by treating the collisional width, shift, and asymmetry parameter of the pressure-broadening component of the line profile as parameters, depending on the speed of the emitter. The full line shape, after performing the velocity average using Maxwellian distribution, is then given either by a ''speed-dependent Voigt profile'' (SDVP) first derived by Berman [11] for the pure impact case, i.e., when the collision duration time is neglected or by a ''speed-dependent asymmetric Voigt profile'' (SDAVP) given by Harris *et al.* [15] for the case when the finite duration of collisions is taken into account.

Apart from pressure broadening, the speed-dependent effects and, in particular, the speed dependence of the Lorentzian width may in some cases lead to the narrowing of the line as well. This effect, which was described by Berman [11] and Ward *et al.* [12] and tested by several authors [15–22], is manifested by the decrease with the increase of perturbing gas density of the Doppler width determined from the fits of theoretical profiles such as VP or AVP to experimental profiles. Another feature of speed-dependent effects on spectral lines is that they may give rise to an asymmetry of line shapes even in the case when the finite duration of collisions may be neglected. Such an effect results from the speed dependence of pressure shift of the line as was experimentally demonstrated by Farrow *et al.* [23]. It must be emphasized that because of the similarity between contributions from collision duration time and speed-dependent effects, extreme care is needed in any quantitative interpretation of

 

asymmetry of pressure-broadened spectral line shapes.

It must also be noted that aside from the narrowing caused by speed-dependent effects, another type of collisional narrowing may occur due to the velocity-changing collisions. This phenomenon was originally described by Dicke [24] who has shown that if the mean free path of the emitter between two successive collisions becomes smaller than the wavelength of the radiation, then the Doppler width is appreciably reduced. This effect, which is similar in origin to the Mössbauer effect, is known as Dicke narrowing. Two theoretical models of the translational motion have been used to describe the profiles of Dicke-narrowed spectral lines. These are the soft-collision model developed by Galatry [25] and hard-collision model given by Nelkin and Ghatak [26]. In recent years, these two models served as starting points for several researchers who developed theoretical approaches to take into account the simultaneous influence of Dicke narrowing, correlation between velocity changing and dephasing collisions [27,28], and speed dependence of collisional parameters [29–35], as well as collision duration time [14,36,37] on the resultant line shape.

In a series of experiments in this laboratory [22,38–40] the pressure broadening and shift of the $^{114}$Cd 326.1-nm ($5\,^1S_0$–$5\,^3P_1$) intercombination line perturbed by He, Ne, Ar, Kr, and Xe have been studied by means of classical emission spectroscopy using a pressure-scanned Fabry-Perot interferometer. It should be noted that due to the weakness of the fluorescence signal and small transmission of the Fabry-Perot interferometer (its inherent feature), such line-shape measurements were possible only for the perturbing gas pressures less than 100 Torr at room temperature.

Our earlier work [22] on the Cd-Xe system performed with a pressure-scanned Fabry-Perot interferometer (FPI) indicated that the simple Voigt function that is a convolution of Lorentzian and Gaussian components is inadequate because the Doppler width obtained from the Voigt analysis was found to decrease markedly with increasing xenon pressure. This result is a manifestation of the correlation between the collision and Doppler broadening. We should emphasize, however, that departures from the Voigt profile are difficult to observe by means of classical spectroscopic methods since the effects are small, and even with high-resolution instruments such as FPI the instrumental profile is not negligible. In particular, our numerical simulations have shown that for real FPI it is practically impossible to observe the collision-time asymmetry because this effect is totally obscured by the periodic instrumental function of FPI.

The above limitation as well as a small pressure range (below 100 Torr) and rather poor, (especially for higher pressures) signal-to-noise ratio did not allow us in our previous work to register and analyze the collision-time asymmetry for the Cd-Xe system. It should be noted, however, that in our recent study [41] on the influence of Kr on the 326.1-nm $^{114}$Cd line we were able to detect the collision-time asymmetry using a classical absorption spectroscopy method. The spectral resolution of the apparatus used in that study was too low to perform any quantitative analysis of the role of speed-dependent effects in the formation of resulting profiles.

In the present paper, we report results of detailed studies of the shapes of the 326.1-nm $^{114}$Cd line perturbed by xenon gas that were performed using a laser-induced fluorescence technique. A good signal-to-noise ratio and negligible instrumental profile (that of a ring dye laser is about 1 MHz) enable us to fit the line shapes in considerable detail and record deviations from the ordinary Voigt profile that can be ascribed to both the collision-time asymmetry and speed-dependent effects.

The measured line shapes are then analyzed in terms of the speed-dependent asymmetric Voigt profile and the pressure-broadening, shift, and asymmetry coefficients are determined and compared with those calculated on the basis of some interaction potentials that are available for Cd-Xe. The effects of velocity-changing collisions are also investigated using a model that describes both the speed-dependent effects and collisional narrowing processes [37].

## II. EXPERIMENTAL SETUP

To avoid the hyperfine and isotopic structure of the Cd 326.1-nm line, the measurements were performed using the $^{114}$Cd isotope. The sidearm quartz cells containing cadmium were filled with xenon and cutoff from the vacuum system. The xenon pressure was varied between 5 and 368 Torr at room temperature. The cells were situated in the special multisection oven, enabling the independent temperature stabilization of the cell and its sidearm up to 1 K. During the measurement, the temperature of the cell was kept constant at 724 K, while the sidearm was kept at temperature of 440 K.

The line shape of the cadmium 326.1-nm line was registered using a digital laser spectrometer described elsewhere [43]. The intensity of the fluorescence signal as the laser frequency was scanned across the line was measured by a thermoelectrically cooled photomultiplier working in the photon counting mode. An actively stabilized single-frequency Coherent 899-21 ring dye laser equipped with an intracavity frequency doubler, operating on 4-(dicyanomethylene)-2-methyl-6-(4-dimethylaminostyryl)-4H-pyran dye, was pumped by an INNOVA-400 argon-ion laser. The ring laser provided single-mode UV output continuously tunable for up to 60 GHz with line width about 1 MHz. Frequency calibration of the ring laser was performed using its fundamental (red) line directed to a confocal FPI with a free spectral range of 1.5 GHz and the 100-cm-long iodine cell operated at 35 °C. The FPI transmission peaks and $I_2$ absorption spectrum were recorded simultaneously with the fluorescence signal for frequency calibration. The laser UV beam incident on the cell was linearly polarized in the vertical direction, and the collection optics arm, perpendicular to the laser beam direction, contained a linear polarizer set at the ''magic angle'' (rotated 54.7$^o$ from the vertical), so that the collection optics system was insensitive to effects due to anisotropy of fluorescence (see, e.g., [17,44]). Photon counting was performed by an electronic system built in the computer application for measurements and control standard described elsewhere [38]. All of the data, fluorescence signal, laser UV output power, FPI transmission peaks,

and $I_2$ absorption spectrum, were acquired with a PC computer for further evaluation.

## III. LINE SHAPE

### A. Speed-dependent asymmetric Voigt profile

As was mentioned in the Introduction, the shape of a pressure-broadened line can be described by the sum of Lorentzian and dispersion distributions. If emitters move with velocity $\vec{v}_E$, this profile can be written in the following form:

$$I(\tilde{\nu},\vec{v}_E)=\frac{1}{\pi}\frac{[\gamma_L(v_E)/2]+\chi(v_E)[\tilde{\nu}-\tilde{\nu}_0(\vec{v}_E)-\Delta(\vec{v}_E)]}{[\gamma_L(v_E)/2]^2+[\tilde{\nu}-\tilde{\nu}_0(\vec{v}_E)-\Delta(\vec{v}_E)]^2}, \tag{1}$$

where $\gamma_L(v_E)$, $\Delta(v_E)$, $\chi(v_E)$ denote the speed-dependent Lorentzian width (FWHM), shift, and collision-time asymmetry parameter, respectively, and

$$\tilde{\nu}_0(\vec{v}_E)=\tilde{\nu}_0+\frac{\vec{k}\cdot\vec{v}_E}{2\pi c} \tag{2}$$

is the unperturbed wave number $\tilde{\nu}_0$ of the emitted line modified by the Doppler shift. Here $\vec{k}$ is the wave vector of the emitted radiation and $c$ is the speed of light.

In the general case, the speed-dependent Lorentzian width and shift can be evaluated from the following expression [1,2,14,12]:

$$\frac{\gamma_L(v_E)}{2}+i\Delta(v_E)=\frac{N}{c}\int d^3\vec{v}_{EP}f_{m_P}(\vec{v}_E+\vec{v}_{EP})v_{EP}\int_0^{+\infty}d\rho\rho \times\{1-\langle U_{ii}(+\infty,-\infty) \times U_{ff}^{-1}(+\infty,-\infty)\rangle_{Ang.Av.}\}. \tag{3}$$

Here $N$ is perturber density, $\rho$ is the impact parameter and $f_{m_P}(\vec{v}_P)$ is the Maxwellian distribution of velocities $\vec{v}_P$ of perturbers with mass $m_P$ connected with emitter velocity $\vec{v}_E$ and the relative perturber-emitter velocity $\vec{v}_{EP}$ by following the relation $\vec{v}_P=\vec{v}_E+\vec{v}_{EP}$. The product of time-evolution operators for the initial and final states averaged over angular coordinates $\langle U_{ii}(t_2,t_1)U_{ff}^{-1}(t_2,t_1)\rangle_{Ang.Av.}$ is dependent on $v_{EP}$ and $\rho$. In a good approximation, $\chi(v_E)$ can be evaluated from the expression derived in our earlier papers [10,14]:

$$\chi(v_E)=2\pi N\int d^3\vec{v}_{EP}f_{m_P}(\vec{v}_E+\vec{v}_{EP})v_{EP}\int_0^{+\infty}d\rho\rho\int_{-\infty}^{+\infty}dt_0 \times\mathrm{Im}\{1+\langle U_{ii}(+\infty,-\infty)U_{ff}^{-1}(+\infty,-\infty) -U_{ii}(t_0,-\infty)U_{ff}^{-1}(t_0,-\infty)-U_{ii}(+\infty,t_0) \times U_{ff}^{-1}(+\infty,t_0)\rangle_{Ang.Av.}\}. \tag{4}$$

Hereafter we use the first-order approximation in which $\cos[\chi(v_E)]\approx 1$ and $\sin[\chi(v_E)]\approx\chi(v_E)$.

To obtain the resulting line shape, Eq. (1) should be averaged over the Maxwellian distribution $f_{m_E}(\vec{v}_E)$ of velocities of emitters with mass $m_E$. The averaged profile can be written in the following form:

$$I(\tilde{\nu})=\int d^3\vec{v}_E\,f_{m_E}(\vec{v}_E)I(\tilde{\nu},\vec{v}_E). \tag{5}$$

Following Harris *et al.* [15] (see also [14]) after performing the integration over $\vec{v}_E$ using the reduced emitter speed $x=v_E/v_{m_E}$ (where $v_{m_E}=\sqrt{2k_BT/m_E}$ is the most probable speed of the emitter, $T$ is the gas temperature, and $k_B$ is Boltzmann's constant) the resultant line shape that takes into account both the collision-time asymmetry and speed-dependent effects can be written in the form of the SDAVP:

$$I_{SDAVP}(\tilde{\nu})=\frac{2}{\pi^{3/2}\tilde{\nu}_D}\int_{-\infty}^{+\infty}dx e^{-x^2}x\left\{\arctan[A(x)] +\frac{\langle\chi\rangle B_A(x;\alpha)}{2}\ln[1+A^2(x)]\right\}, \tag{6}$$

where

$$A(x)=\frac{\tilde{\nu}-\tilde{\nu}_0-\langle\Delta\rangle B_S(x;\alpha)+x\tilde{\nu}_D}{\langle\gamma_L\rangle B_W(x;\alpha)/2}. \tag{7}$$

Here, $\tilde{\nu}_D=\tilde{\nu}_0 v_{m_E}/c$ is proportional to the Doppler width $\gamma_D$ (FWHM), i.e., $\tilde{\nu}_D=\gamma_D/(2\sqrt{\ln 2})$. Functions $B_W(x;\alpha)$, $B_S(x;\alpha)$, and $B_A(x;\alpha)$ are defined by

$$B_W(x;\alpha)=\frac{\gamma_L(xv_{m_E})}{\langle\gamma_L\rangle}, \tag{8}$$

$$B_S(x;\alpha)=\frac{\Delta(xv_{m_E})}{\langle\Delta\rangle}, \tag{9}$$

$$B_A(x;\alpha)=\frac{\chi(xv_{m_E})}{\langle\chi\rangle}, \tag{10}$$

the reduced Lorentzian width (FWHM), reduced pressure shift, and reduced collision-time asymmetry (CTA) parameter, respectively [14,12,13]. The quantities $\langle\gamma_L\rangle$, $\langle\Delta\rangle$ and $\langle\chi\rangle$ in the denominators of Eqs. (8)–(10) are the Lorentzian width, pressure shift, and CTA parameter averaged over the Maxwellian distribution $f_{m_E}(\vec{v}_E)$ of the emitter velocities $\vec{v}_E$ and they can be written in the following way:

$$\langle\gamma_L\rangle=\int d^3\vec{v}_E\,f_{m_E}(\vec{v}_E)\gamma_L(v_E), \tag{11}$$

$$\langle\Delta\rangle=\int d^3\vec{v}_E\,f_{m_E}(\vec{v}_E)\Delta(v_E), \tag{12}$$

$$\langle\chi\rangle=\int d^3\vec{v}_E\,f_{m_E}(\vec{v}_E)\chi(v_E). \tag{13}$$

It should be noted that in the limiting cases, the SDAVP profile, Eq. (6), becomes identical with functions used in traditional line-shape analysis (see also Ref. [14]). For instance, the neglect of speed-dependent effects that is justified for small $\alpha$ values leads to the AVP simply by putting $B_W(x;\alpha)=B_S(x;\alpha)=B_A(x;\alpha)=1$ in Eqs. (6) and (7). On the other hand, the neglect of the collision-time asymmetry leads to the SDVP [11] simply by putting $\chi=0$ in Eq. (6). The neglect of both the above effects leads to the ordinary VP.

### B. Adiabatic approximation

In order to adapt the above approach to the analysis of experimental line shapes for Cd-Xe systems, the interatomic potentials involving the Cd ground ($5s^2\,{}^1S_0$) and the excited ($5s5p\,{}^3P_1$) states must first be known. The interaction between ground-state atoms Cd($5s^2\,{}^1S_0$)+Xe($5p^6\,{}^1S_0$) is described by a single potential curve corresponding to the $X^1 0^+$ molecular state. During the collision of the Cd atom excited to the $5s5p\,{}^3P_1$ state, two molecular states labeled as $A^3 0^+$ and $B^3 1$ are formed that are described by two different potential curves. The broadening and shift of the Cd 326.1 nm intercombination line ($5s5p\,{}^3P_1$-$5s^2\,{}^1S_0$) is thus the result of contributions from the $A^3 0^+$-$X^1 0^+$ and $B^3 1$-$X^1 0^+$ transitions.

In the adiabatic approximation for the Cd 326.1-nm line perturbed by Xe, the product of time-evolution operators averaged over angular coordinates can be written as [10,22]

$$\langle U_{ii}(t_2,t_1)U_{ff}^{-1}(t_2,t_1)\rangle_{Ang.Av.} = \frac{1}{3}\exp[-i\,\eta_{A-X}(t_2,t_1)]+\frac{2}{3}\exp[-i\,\eta_{B-X}(t_2,t_1)], \tag{14}$$

where $\eta_{A-X}(t_2,t_1)$ and $\eta_{B-X}(t_2,t_1)$ are the phase shifts for the $A^3 0^+$-$X^1 0^+$ and $B^3 1$-$X^1 0^+$ transitions, respectively. These functions are given by the following expression:

$$\eta(t_2,t_1)=\frac{1}{\hbar}\int_{t_2}^{t_1}\Delta V(r(\tau))d\tau, \tag{15}$$

where $\Delta V(r)$ denotes the difference of potentials $V(A^3 0^+)-V(X^1 0^+)$ and $V(B^3 1)-V(X^1 0^+)$, respectively, and $r(\tau)=\sqrt{\rho^2+v_{EP}^2\tau^2}$ is the interatomic distance at time $\tau$.

It should be noted that the use of the semiclassical adiabatic approach and the straight-line approximation in the description of the motion of colliding atoms applied in this work can lead to some errors in the evaluation of collisional width, shift, and asymmetry. However, for isolated lines of neutral atoms of metals perturbed by heavy rare-gas atoms, i.e., for systems like Cd-Xe, it is usually sufficient to use the adiabatic approach with straight-line trajectories [2,3].

### C. Velocity-changing collisions

As we mentioned in the Introduction, the Dicke narrowing resulting due to velocity-changing collisions may contribute to the line shape if the mean free path becomes of the order of the wavelength of the emitted light. This means that the role of the Dicke narrowing increase with the increase of perturbing gas pressure in accordance with theoretical predictions of the soft- [25] and hard- [26] collision model in which the velocity-changing and dephasing collisions are treated as statistically independent events. Rautian and Sobelman [27] have indicated, however, that in many cases, correlation between velocity-changing and dephasing collisions should also be taken into account. Such a correlation gives rise to profiles that in the presence of pressure shift are asymmetric as was experimentally confirmed by Pine [28,33] for rovibrotional lines of HF perturbed by Ar. An important feature of this correlation is that they can lead to the marked reduction of the Dicke narrowing or even its complete elimination.

In order to estimate the contribution of the Dicke narrowing to the shape of the 326.1-nm Cd line perturbed by Xe, we used in this work a unified formula presented recently [37] on the basis of the approaches given by Ciuryło [14] and Pine [33]. That formula is unified in the sense that it describes the ordinary pressure broadening due to dephasing collisions with the inclusion of the finite duration of those collisions, speed-dependent effects, and Dicke narrowing, as well as correlation between dephasing and velocity-changing collisions. To simplify the calculations, we used the hard-collision model of the Dicke narrowing given by Nelkin and Ghatak [26]. The unified formula given in Ref. [37] takes then a form called the correlated speed-dependent asymmetric Nelkin-Ghatak profile (CSDANGP) that represents an asymmetric version of the correlated speed-dependent Nelkin-Ghatak profile derived by Pine [33].

The most important quantity in the hard-collision model is the effective frequency of velocity-changing collisions which is inversely proportional to the diffusion coefficient $D$ for the emitter surrounded by the perturbing gas. Unfortunately, for Cd-Xe, neither experimental nor theoretical data on $D$ are available. Therefore the accurate analysis of the influence of the Dicke narrowing on the Cd 326.1-nm line perturbed by Xe is not possible at present. Nevertheless, using the CSDANGP formula with coefficients evaluated from simplified treatments of the diffusion in binary systems [47] for the Cd-Xe interatomic potentials calculated by Czuchaj and Stoll [42], we performed simulations of the profiles of the Xe-broadened 326.1-nm Cd line. The main conclusion of these simulations is that for Cd-Xe, the extent of the Dicke narrowing of the Doppler component of the 326.1-nm line for the highest Xe pressure used in the present experiment is below $4\times10^{-3}$ cm$^{-1}$. Moreover, it will be seen that we have shown in the next section that no additional decrease of the Doppler width caused by the Dicke narrowing is observed in our experiment. We can thus conclude that in our case, Dicke narrowing makes a negligible contribution to the width and shape of the 326.1-nm line. Therefore, in the following we perform the analysis of our experimental data using the SDAVP formula, Eq. (6), in which Dicke narrowing is neglected. We should also mentioned that for systems like Ca perturbed by rare-gas atoms [16–18] as well as for some spectral lines of Ne and Ar perturbed by Ne [20,21],

the observed line shapes were successfully interpreted in terms of SDAVP or SDVP expressions.

## IV. DATA ANALYSIS

In order to examine the role of the collision-time asymmetry and speed-dependent effects in the production of the total line shape, we fitted the following profiles to our experimental data: ordinary Voigt profile $I_{VP}(\tilde{\nu})$, speed-dependent Voigt profile $I_{SDVP}(\tilde{\nu})$, asymmetric Voigt profile $I_{AVP}(\tilde{\nu})$, and speed-dependent asymmetric Voigt profile $I_{SDAVP}(\tilde{\nu})$. The best-fit procedure was performed using a least-squares algorithm for nonlinear parameters due to Marquardt [45]. Our numerical fit to $I_{VP}(\tilde{\nu})$ as well as to $I_{SDVP}(\tilde{\nu})$ allowed three parameters to vary: the Gaussian width $\gamma_D$, the Lorentzian width $\langle \gamma_L \rangle$, and the line shift $\langle \Delta \rangle$. For asymmetric profiles $I_{AVP}(\tilde{\nu})$ and $I_{SDAVP}(\tilde{\nu})$, we also fitted the asymmetry parameter $\langle \chi \rangle$. The $B_W(x;\alpha)$ and $B_S(x;\alpha)$ functions used in the SDVP and SDAVP were calculated from Eqs. (8) and (9), using for Cd-Xe interaction the potentials recently reported by Czuchaj and Stoll [42]. In the SDAVP the $B_A(x;\alpha)$ function was taken to be equal to one (see Sec. IV C).

Figure 1(a) shows an example of the shape of the 326.1-nm $^{114}$Cd line perturbed by Xe at 203 Torr at room temperature. The best-fit profile $I_{SDAVP}(\tilde{\nu})$ is plotted as the solid line. In order to examine the quality of the fits we used the weighted differences of the intensities

$$D_\sigma(\tilde{\nu}) = \frac{I_{expt}(\tilde{\nu}) - I_{theor}(\tilde{\nu})}{\sqrt{I_{theor}(\tilde{\nu})}}, \tag{16}$$

between experimental (measured) $I_{expt}(\tilde{\nu})$ and theoretical (fitted) $I_{theor}(\tilde{\nu})$ profiles. In Fig. 1(b) we plotted these differences for the case when $I_{theor}(\tilde{\nu})$ profile was given by the ordinary Voigt profile $I_{VP}(\tilde{\nu})$. We can see systematic departures from zero in the line core as well as on line wings that can be regarded as a manifestation of the line asymmetry. Figure 1(c) shows the differences for the case when $I_{theor}(\tilde{\nu})$ is given by the speed-dependent Voigt profile $I_{SDVP}(\tilde{\nu})$. The systematic departures are still present on the line wings, while in the line core the quality of the fit is better. For $I_{theor}(\tilde{\nu})$ given by the asymmetric Voigt profile $I_{AVP}(\tilde{\nu})$ [Fig. 1(d)], an improvement of the fit was obtained only on line wings. Finally, Fig. 1(e) shows the differences for the case when $I_{theor}(\tilde{\nu})$ is given by the speed-dependent asymmetric Voigt profile $I_{SDAVP}(\tilde{\nu})$. As can be seen in this case, the values of the differences are spread uniformly about zero, which confirms the goodness of the fit. We can thus conclude that in the case of the Cd-Xe system, both the collision-time asymmetry and speed-dependent effects have a noticeable influence on the profile of the 326.1-nm line.

In the following, we are going to focus our attention on the problem of how to distinguish these two effects that both can lead to asymmetry of the profile. Therefore in our analysis described in following sections we use the AVP and SDAVP profiles only.

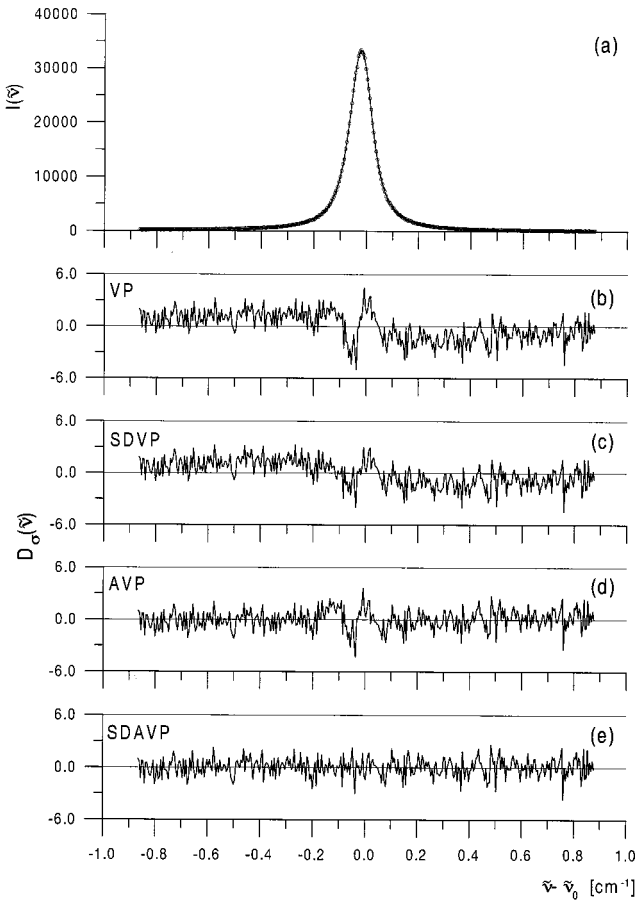


FIG. 1. (a) The shape of the Cd 326.1-nm line perturbed by Xe at pressure 203 Torr: experimental points together with the best-fit SDAVP (with Czuchaj and Stoll potential) (full curve) and weighted differences $D_\sigma(\tilde{\nu})$ between experimental and the fitted (b) Voigt profile (VP), (c) speed-dependent Voigt profile (SDVP), (d) asymmetric Voigt profile (AVP), and (e) speed-dependent asymmetric Voigt profile (SDAVP), respectively.

### A. Doppler broadening

Figure 2 shows the values of the Doppler width $\gamma_D$ of the 326.1-nm Cd line perturbed by xenon determined from the best fit of the AVP to experimental data, plotted against the pressure of Xe. As can be seen, the Doppler width is found to decrease markedly with increasing Xe pressure. This can be interpreted as a manifestation of the Doppler-collision correlation effects and it is in agreement with theoretical predictions due to Berman [11] and Ward *et al.* [12] and with previous experimental observations [16,18,20–22] and our numerical simulations.

In Fig. 2 we also plotted the values of the Doppler width $\gamma_D$ determined from the best fit of the SDAVP to the experimental data. It should be noted that evaluation of the SDAVP requires the knowledge of the dependence of the emitter-

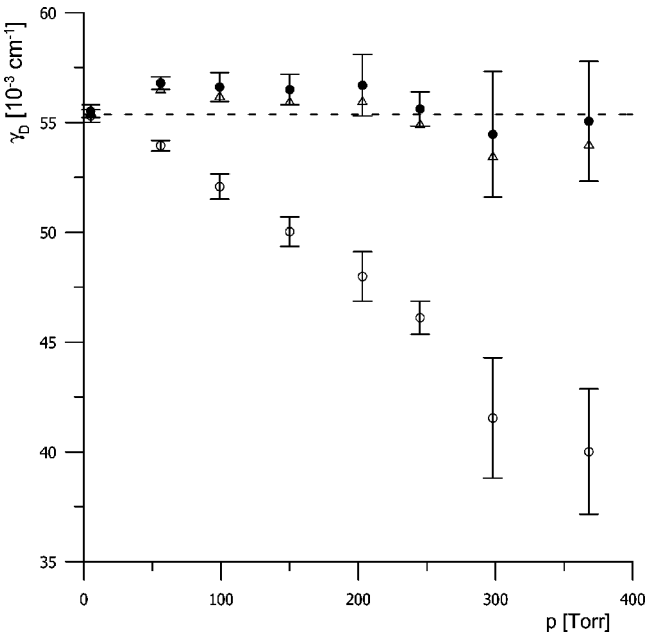


FIG. 2. Plots of the Doppler width $\gamma_D$ of the 326.1-nm Cd line perturbed by xenon determined from the best fit of the AVP (open circles) and SDAVP [for van der Waals (triangles) and Czuchaj and Stoll (filled circles) potentials] to the experimental data, against the pressure of Xe. Dashed line, theoretical Doppler width corresponding to the cell temperature (724 K). Error bars indicate the value of the standard deviation.

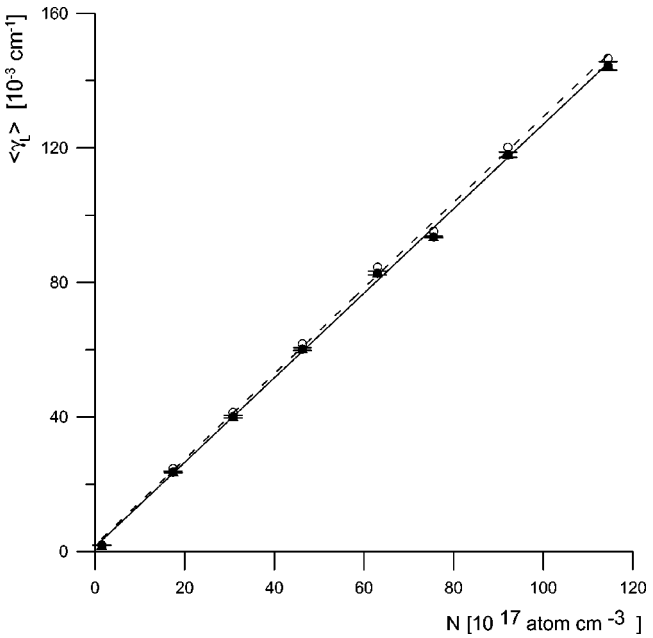


FIG. 3. Plots of the Lorentzian width $\langle \gamma_L \rangle$ of the 326.1-nm Cd line determined from the best fit of the AVP (open circles and dashed line) and SDAVP [for van der Waals (triangles and dashed-and-dotted line) and Czuchaj and Stoll (filled circles and solid line) potentials] to the experimental data against the xenon density *N*. Error bars indicate the value of the standard deviation. For the clarity of the figure, we plotted the error bars only for the SDAVP (with Czuchaj and Stoll potential). For two other fits the error values were of the same magnitude.

perturber interaction potential $V(r)$ on the interatomic distance $r$. We performed the best-fit procedure for two cases: in the first case we assumed this interaction in the form of the van der Waals potential and in the second case we used the numerical potentials calculated by Czuchaj and Stoll [42]. In the first case, i.e., for $\Delta V(r) = -C_6/r^6$, the $B_W(x;\alpha)$ and $B_S(x;\alpha)$ functions can be evaluated from the analytical expression [12]

$$B_W(x;\alpha) = B_S(x;\alpha) = (1+\alpha)^{-0.3} M(-0.3,1.5,-\alpha x^2), \tag{17}$$

where $M(a,b,z)$ is the confluent hypergeometric function. In the second case these functions must be evaluated from Eqs. (8) and (9). In our fits we have used in both cases $B_A(x;\alpha) = 1$ (see Sec. IV C)

As can be seen for SDAVP there is practically no dependence of the Doppler width $\gamma_D$ on the Xe pressure. The average Doppler widths determined for SDAVP using the van der Waals and Czuchaj-Stoll [42] potentials are found to be $55.4(1.8)\times 10^{-3}$ cm$^{-1}$ and $55.9(1.7)\times 10^{-3}$ cm$^{-1}$, respectively. These values agree very well with theoretical Doppler width $55.4\times 10^{-3}$ cm$^{-1}$ corresponding to the cell temperature $T = 724$ K.

### B. Pressure broadening and shift

Figures 3 and 4 show the plots of the Lorentzian width $\langle \gamma_L \rangle$ and shift $\langle \Delta \rangle$ determined from the best fit of AVP and SDAVP (with van der Waals and Czuchaj-Stoll [42] potentials) to our experimental profiles against the density number

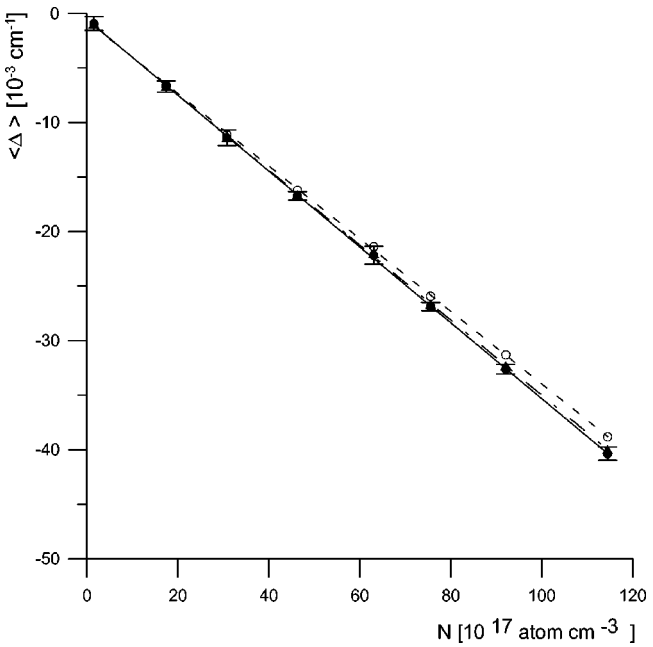


FIG. 4. Plots of the shift $\langle \Delta \rangle$ of the 326.1-nm Cd line determined from the best fit of the AVP and SDAVP to the experimental data against the xenon density *N*. (Notations as in Fig. 3.).

TABLE I. Comparison of experimental values of the $\beta$, $\delta$ (in units $10^{-20}$ cm$^{-1}$/atom cm$^{-3}$), and $\kappa$ (in units $10^{-21}$/atom cm$^{-3}$) coefficients with those calculated for different interatomic potentials. For experimental data the values of standard deviations are given.

| Experimental values | $\beta_{expt}$ | $\delta_{expt}$ | $\kappa_{expt}$ |
|---|---|---|---|
| Brym *et al.* [23] ($p<80$ Torr) | 1.223(19) | −0.304(31) | |
| This work AVP | 1.273(7) | −0.333(2) | −1.42(8) |
| This work SDAVP-vdW | 1.258(6) | −0.344(2) | −1.16(7) |
| This work SDAVP-CS | 1.257(6) | −0.348(2) | −1.08(7) |
| Theoretical values | $\beta_{theor}$ | $\delta_{theor}$ | $\kappa_{theor}$ |
| van der Waals | 1.127 | −0.408 | −1.16 |
| Morse | 1.101 | −0.221 | −0.89 |
| Czuchaj-Stoll [43] | 1.330 | −0.322 | −1.15 |

$N$ of xenon. As it is seen, the shift is toward the red, and both $\langle\gamma_L\rangle$ and $\langle\Delta\rangle$ are linearly dependent on the density. From the slopes of these linear dependencies, the pressure-broadening $\beta=\langle\gamma_L\rangle/N$ and shift $\delta=\langle\Delta\rangle/N$ coefficients were determined and listed in Table I. They are marked ''This work AVP,'' ''This work SDAVP-vdW,'' and ''This work SDAVP-CS,'' respectively.

It is seen that our experimental values of $\beta$ and $\delta$ determined from these three fitting procedures are different although they are close to each other. The broadening coefficients obtained by the speed-dependent analysis are only slightly lower (about 1%) than those resulting from the asymmetric Voigt profile analysis. Unlike the broadening, the pressure shift coefficients obtained by the speed-dependent analysis are slightly higher (about 4%) than those obtained for asymmetric Voigt profile.

### C. Line asymmetry

Figure 5 shows the plot of the asymmetry parameter $\langle\chi\rangle$ determined from the best fit of AVP and SDAVP (with van der Waals and Czuchaj-Stoll [42] potentials) to our experimental profiles, against the density number $N$. As it is seen, the asymmetry parameter is linearly dependent on the density. From the slope of the best-fit straight line, the asymmetry coefficients $\kappa=\chi/N$ were determined and listed in Table I. It is seen that our experimental values of $\kappa$ coefficients obtained by speed-dependent analysis for van der Waals and Czuchaj-Stoll potentials are close each other, but they are lower by about 20% than those resulting from the asymmetric Voigt profile analysis.

It should be noted that the $B_A(x;\alpha)$ function may be represented in an analytic form only in some cases, for instance, for inverse-power potentials [13]. For the van der Waals potential, this function is given by the following expression [13]:

$$B_A(x;\alpha)=(1+\alpha)^{0.3}M(0.3,1.5,-\alpha x^2). \qquad (18)$$

In the general case, for instance, when potentials are given in the numerical form, this function must be evaluated numerically using Eq. (10). However, numerical calculation of the $B_A(x;\alpha)$ function from Eq. (10) is much more time consuming than calculations of $B_W(x;\alpha)$ and $B_S(x;\alpha)$ functions from Eqs. (8) and (9), respectively.

We investigated the influence of the $B_A(x;\alpha)$ function on the results obtained from the fit of the SDAVP to experimental profiles. To carry out this investigation, we used the $B_A(x;\alpha)$ function evaluated from Eq. (18); we have also studied the case when we can assume that $B_A(x;\alpha)=1$. In these two cases, we used $B_W(x;\alpha)$ and $B_S(x;\alpha)$ given by Eq. (17). The values of the parameters $\gamma_D$, $\langle\gamma_L\rangle$, $\langle\Delta\rangle$, and $\langle\chi\rangle$ obtained from both fits as well as the quality of these fits were the same for all analyzed line shapes. Therefore, in this work all fits of the SDAVP (for both van der Waals and Czuchaj-Stoll [42] potentials) were done assuming $B_A(x;\alpha)=1$. This means that in practice we can neglect the speed dependence of the collision-time asymmetry in our investigations.

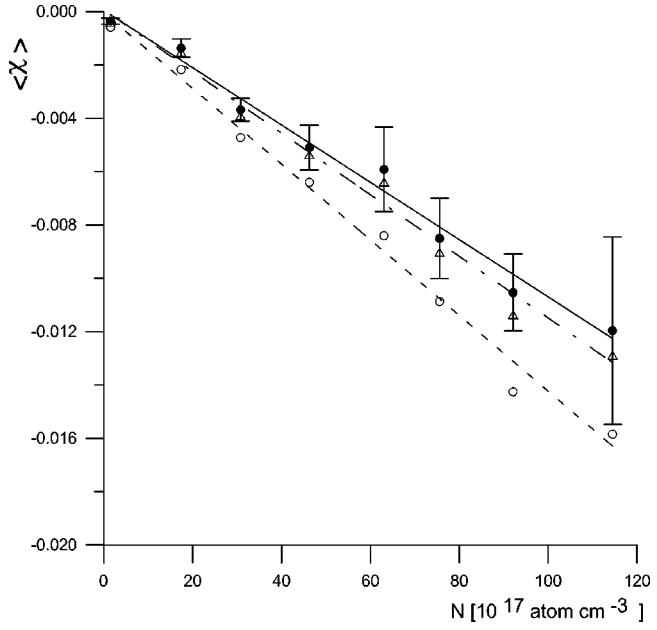


FIG. 5. Plots of the asymmetry parameter $\langle\chi\rangle$ determined from the best fit of AVP and SDAVP to the experimental data against the xenon density $N$. (Notations as in Fig. 3.)

## V. RESULTS AND DISCUSSION

We have shown that the SDAVP, Eq. (6), gives a correct description of our experimental profiles of the $^{114}$Cd 326.1-nm line perturbed by xenon. This means that for the Cd-Xe system the reliable experimental values of the Doppler width can be obtained from the line-shape analysis provided the speed-dependent effects are taken into account. Neglect of the speed dependence of the collisional width and shift leads to some errors in determination of the pressure-broadening, shift, and asymmetry coefficients, which in the case of the Cd-Xe system are estimated to be about 1%, 4%, and 20%, respectively.

The experimental values of pressure-broadening $\beta$, shift $\delta$, and asymmetry $\kappa$ coefficients determined in the course of the present work are listed in Table I. In a previous work [23] from this laboratory, the $\beta$ and $\delta$ coefficients for the 326.1-nm Cd line perturbed by Xe were determined using a classical spectroscopy technique, i.e., by means of a pressure-scanned Fabry-Perot interferometer for the cell temperature $T=468$ K. It seems that the value of the pressure-broadening coefficient reported in Ref. [22] that is equal to $1.319(27)\times10^{-20}$ cm$^{-1}$/atoms cm$^{-3}$ can be affected by a systematic error. This kind of error can be due to the low signal-to-noise ratio for higher perturber pressures as well as strong numerical correlation between parameters representing collisional and Doppler widths in the fitting procedure. Therefore we rejected the values of Lorentzian width and shift corresponding to the highest xenon pressure ($p=102$ Torr) determined in Ref. [22]. The recalculated values of $\beta$ and $\delta$ coefficients are listed in Table I where they are marked ''Brym *et al.* [22] ($p<80$ Torr).'' As it can be seen from Table I there is practically no change of $\beta$ and $\delta$ coefficients with the change of cell temperature from $T=468$ K to $T=724$ K. This result is in agreement with Dietz *et al.* [46] who found the lack of the temperature dependence of the line-shape parameters for cadmium perturbed by helium and argon in the temperature range between 503 K and 663 K.

In order to interpret our experimental data we calculated the theoretical values of pressure broadening $\beta$ and shift $\delta$ coefficients from Eq. (3) for different interaction potentials. We performed the calculation for the Czuchaj and Stoll [42] numerical potential as well as for two potentials derived from experimental data, i.e., for van der Waals and Morse potentials with the same constants as used in Ref. [22]. The values of $\beta$ and $\delta$ coefficients evaluated for these potentials are listed in Table I and marked as ''Czuchaj-Stoll [42],'' ''van der Waals,'' and ''Morse,'' respectively. As can be seen from Table I, our experimental values of $\beta$ and $\delta$ are in reasonable agreement with theoretical ones calculated on the basis of the Czuchaj-Stoll [42] potential.

The experimental values of collision-time asymmetry coefficients $\kappa$ determined in the course of the present work are listed in Table I where they are compared with theoretical values. Our careful tests have shown that in the case of the van der Waals potential the values of the asymmetry parameter calculated in the framework of the unified Franck-Condon treatment [3,6] are very close to that obtained from formula (4) corresponding to the Anderson-Talman approach [4,5] (see the Appendix). It should be noted, however, that Eq. (4) is more convenient for numerical application, especially in the case of averaging over Maxwellian distribution of velocities than other known expressions [6,7]. Therefore theoretical values of asymmetry coefficient $\kappa$ were calculated from Eqs. (13) and (4) for the Czuchaj and Stoll [42] numerical potential as well as for van der Waals and Morse potentials with the same constants as those used in our previous paper [22] on the Cd-Xe system. As can be seen from Table I good agreement between our experimental and theoretical values of the asymmetry coefficient $\kappa$ takes place for the Czuchaj-Stoll [42] as well as for the van der Waals potential. The poor agreement is obtained, however, for the Morse potential.

## VI. CONCLUSION

We have presented a detailed analysis of our experimental profiles of the 326.1-nm $^{114}$Cd line perturbed by Xe that clearly establish the existence of the collision-time asymmetry in the near-wing region. With our increased experimental precision compared to previous results [22], we have shown that for the Cd-Xe system, the neglect of the speed dependence of the collisional width and shift may cause errors in the values of the Doppler width and collision-time asymmetry parameter determined from the line-shape analysis. On the other hand, the speed dependence of the collision-time asymmetry and Dicke narrowing were found to play a marginal role.

The comparison of pressure broadening, shift, and asymmetry coefficients determined in this experiment with coefficients calculated on the basis of the adiabatic semiclassical approach shows reasonable agreement between experimental and theoretical values obtained for numerical potentials calculated by Czuchaj and Stoll [42]; experimental and theoretical values differ by a few percent. A better agreement cannot be expected from adiabatic calculations. A poor agreement between experimental and theoretical values was obtained for the Morse potential. Moreover, we have shown that for Cd-Xe system an expression derived in Ref. [10] is suitable to describe the collision-time asymmetry in the near-wing region.

## ACKNOWLEDGMENTS

The authors wish to express their gratitude to Professor E. Czuchaj for making available numerical values of potentials. This work was supported by Grant No. 673/PO3/96/10 (2 PO3B 005 10) from the State Committee for Scientific Research.

## APPENDIX

In the case when the difference of potentials can be written in an inverse-power form $\Delta V(r)=\Delta C_q/r^q$, we can write on the basis of Eqs. (13) and (4) that

$$\chi = NK_q \,\mathrm{sgn}(\Delta C_q) \int d^3\vec{v}_{EP} f_\mu(\vec{v}_{EP}) \left[\frac{|\Delta C_q|}{\hbar v_{EP}}\right]^{3/(q-1)}, \tag{A1}$$

where $f_\mu(\vec{v}_{EP})$ is the Maxwellian distribution of relative perturber-emitter velocities $\vec{v}_{EP}$ and $\mu = m_E m_P/(m_E+m_P)$ is the reduced mass for perturber-emitter system. The constant $K_q$ can be evaluated from the following expression:

$$K_q = \int_0^{+\infty} dz\, z^2 \int_{-\infty}^{+\infty} dx\, \mathrm{Im}\{[1-e^{-iz^{1-q}n_q(x,-\infty)}] \times [1-e^{-iz^{1-q}n_q(+\infty,x)}]\}, \tag{A2}$$

where

$$n_q(x_2,x_1) = \int_{x_1}^{x_2} \frac{dy}{(1+y^2)^{q/2}} \tag{A3}$$

and $x$, $y$, and $z$ are dimensionless variables.

The expression for the constant $K_q$ can be rewritten in the form of the product of two integrals

$$K_q = G_q H_q, \tag{A4}$$

where

$$G_q = \int_{-\infty}^{+\infty} dx [n_q(+\infty,x)^{3/(q-1)} + n_q(x,-\infty)^{3/(q-1)} - n_q(+\infty,-\infty)^{3/(q-1)}], \tag{A5}$$

and

$$H_q = \int_0^{+\infty} dx\, x^2 \sin(x^{1-q}). \tag{A6}$$

For the van der Waals potential $(q=6)$ we have

$$n_6(x_2,x_1) = \frac{3}{8}\arctan(x_2) + \frac{x_2(2x_2^2+5)}{8(x_2^2+1)^2} - \frac{3}{8}\arctan(x_1) - \frac{x_1(2x_1^2+5)}{8(x_1^2+1)^2}. \tag{A7}$$

Using Eq. (A4) and performing numerical integration, we obtain in this case $K_6 = 2.717\,71$. This value differs from the value 2.63 given by Traving [5] who corrected a result of Anderson and Talman [4]. On the other hand, our $K_6$ value is the same as that obtained earlier in Ref. [6].


[1] M. Baranger, Phys. Rev. **111**, 494 (1958).
[2] N. Allard and J. Kielkopf, Rev. Mod. Phys. **54**, 1103 (1982).
[3] J. Szudy and W. E. Baylis, Phys. Rep. **266**, 127 (1996).
[4] P. W. Anderson and J. D. Talman (unpublished); (unpublished).
[5] G. Traving, *Uber die Theorie der Druckverbreiterung von Spektrallinien* (G. Braun, Kalsruhe, 1960).
[6] J. Szudy and W. E. Baylis, J. Quant. Spectrosc. Radiat. Transf. **15**, 641 (1975); **17**, 681 (1977).
[7] A. Royer, Acta Phys. Pol. A **54**, 805 (1978).
[8] B. N. I. Al-Saqabi and G. Peach, J. Phys. B **20**, 1175 (1987).
[9] P. S. Julienne and F. H. Mies, Phys. Rev. A **34**, 3792 (1986).
[10] R. Ciuryło, J. Szudy, and R. S. Trawiński, J. Quant. Spectrosc. Radiat. Transf. **57**, 551 (1997).
[11] P. R. Berman, J. Quant. Spectrosc. Radiat. Transf. **12**, 1331 (1972).
[12] J. Ward, J. Cooper, and E. W. Smith, J. Quant. Spectrosc. Radiat. Transf. **14**, 555 (1974).
[13] A. Bielski, S. Brym, R. Ciuryło, and J. Jurkowski, Acta Phys. Pol. A **90**, 523 (1996).
[14] R. Ciuryło, Phys. Rev. A **58**, 1029 (1998).
[15] M. Harris, E. L. Lewis, D. McHugh, and I. Shannon, J. Phys. B **17**, L661 (1984).
[16] I. Shannon, M. Harris, D. McHugh, and E. L. Lewis, J. Phys. B **19**, 1409 (1986).
[17] M. Harris, E. L. Lewis, D. McHugh, and I. Shannon, J. Phys. B **19**, 3207 (1986).
[18] E. L. Lewis, *Spectral Line Shapes*, edited by J. Szudy (Ossolineum, Wrocław, 1988), Vol. 5, p. 485.
[19] D. G. McCartan and N. Lwin, J. Phys. B **10**, L17 (1977).
[20] R. Ciuryło, A. Bielski, S. Brym, J. Domysławska, D. Lisak, J. Szudy, and R. S. Trawiński, Acta Phys. Pol. A **96**, 359 (1999).
[21] A. Bielski, S. Brym, R. Ciuryło, and J. Szudy, Eur. Phys. J. D **8**, 177 (2000).
[22] S. Brym, R. Ciuryło, R. S. Trawiński, and A. Bielski, Phys. Rev. A **56**, 4501 (1997).
[23] R. L. Farrow, L. A. Rahn, G. O. Sitz, and G. J. Rosasco, Phys. Rev. Lett. **63**, 746 (1989).
[24] R. H. Dicke, Phys. Rev. **89**, 472 (1953).
[25] L. Galatry, Phys. Rev. **122**, 1218 (1961).
[26] M. Nelkin and A. Ghatak, Phys. Rev. **135**, A4 (1964).
[27] S. G. Rautian and I. I. Sobelman, Usp. Fiz. Nauk **90**, 209 (1966) [Sov. Phys. Usp. **9**, 701 (1967)].
[28] A. S. Pine, J. Chem. Phys. **101**, 3444 (1994).
[29] P. Duggan, P. M. Sinclair, A. D. May, and J. R. Drummond, Phys. Rev. A **51**, 218 (1995).
[30] R. Ciuryło and J. Szudy, J. Quant. Spectrosc. Radiat. Transf. **57**, 411 (1997).
[31] B. Lance, G. Blanquet, J. Walrand, and J. P. Bouanich, J. Mol. Spectrosc. **185**, 262 (1997).
[32] P. Duggan, P. M. Sinclair, R. Berman, A. D. May, and J. R. Drummond, J. Mol. Spectrosc. **186**, 90 (1997).
[33] A. S. Pine, J. Quant. Spectrosc. Radiat. Transf. **62**, 397 (1999).
[34] D. Robert, P. Joubert, and B. Lance, J. Mol. Struct. **517**, 393 (2000).
[35] D. Priem, F. Rohart, J. M. Colmont, G. Wlodarczak, and J. P. Bouanich, J. Mol. Struct. **517**, 435 (2000).
[36] B. Lance and D. Robert, J. Chem. Phys. **111**, 789 (1999).

[37] R. Ciuryło, A. S. Pine, and J. Szudy, J. Quant. Spectrosc. Radiat. Transf. (to be published).
[38] A. Bielski, S. Brym, R. Ciuryło, J. Domysławska, E. Lisicki, and R. S. Trawiński, J. Phys. B **27**, 5863 (1994).
[39] S. Brym, R. Ciuryło, E. Lisicki, and R. S. Trawiński, Phys. Scr. **56**, 541 (1996).
[40] S. Brym and J. Domysławska, Phys. Scr. **52**, 511 (1995).
[41] J. Domysławska, A. Bielski, and R. S. Trawiński, J. Quant. Spectrosc. Radiat. Transf. **61**, 735 (1999).
[42] E. Czuchaj and H. Stoll, Chem. Phys. **248**, 1 (1999).
[43] A. Bielski, R. Ciurylo, J. Domyslawska, D. Lisak, R. S. Trawinski, and J. Wolnikowski, Acta Phys. Pol. A **97**, 1003 (2000).
[44] R. E. Walkup, A. Spielfiedel, D. Ely, W. D. Phillips, and D. E. Pritchard, J. Phys. B **14**, 1953 (1981).
[45] D. W. Marquardt, J. Soc. Ind. Appl. Math. **11**, 431 (1963).
[46] K. J. Dietz, P. Dabkiewicz, H. J. Kluge, T. Kühl, and H. A. Schuessler, J. Phys. B **13**, 2749 (1980).
[47] J. O. Hirschfelder, C. F. Curtiss, and R. B. Bird, *Molecular Theory of Gases and Liquids* (Wiley, New York, 1954).